Probabilistic Performance-Based Optimal Design of Steel Moment-Resisting Frames. II: Applications

Arzhang Alimoradi, A.M.ASCE[1]; Shahram Pezeshk, M.ASCE[2]; and Christopher M. Foley, M.ASCE[3]

Abstract: Design codes are migrating from prescriptive procedures intended to preserve life safety to reliability-based design. All stakeholders are given the opportunity to speak the common language of risk and structural designs can be developed to not only reliably preserve life safety after rare ground motions, but minimize damage after more frequent ground motions (minimize life-cycle costs). A companion paper presents a methodology for using an evolutionary (genetic) algorithm with radial fitness and balanced fitness functions to generate solutions to optimal design problems formulated within a probabilistic performance-based design framework. The present paper outlines application of the automated algorithm to design steel frames with fully restrained and a variety of partially restrained connections. Comparison of optimal designs resulting from application of the algorithm proposed with those found in the literature is made. Detailed discussion of algorithm performance and response of the resulting optimized designs during pushover and time-history analysis is provided.

DOI: 10.1061/(ASCE)0733-9445(2007)133:6(767)

CE Database subject headings: Seismic design; Nonlinear analysis; Connections, semi-rigid; Evolutionary computation; Optimization; Algorithms; Probabilistic methods; Inelastic action.

Introduction

SAC (2000) presents a performance-based design procedure in a reliability format developed under the SAC Joint Venture project for design of steel moment-resisting frame buildings. The basic procedures include probabilistic evaluation of demand and capacity in terms of structural response parameters for different hazard levels and performance objectives. The ratio of demand to capacity is then calculated incorporating the uncertainties to evaluate confidence levels on the probability of experiencing a performance worse than a specified level during an established period of time (e.g., the structure's expected service lifetime). For each performance objective, the minimum level of confidence obtained from consideration of different response parameters controls the design.

A companion to the present paper (Foley et al. 2007) discusses the probabilistic performance-based design method in greater detail and formulates multiple objective optimization problems. Two fitness formulations suitable for application in a genetic algorithm solution to the optimal design problems are discussed: radial fitness and balanced confidence fitness. The present manuscript proceeds with the application of the automated design algorithms developed to a portal frame with partially and fully restrained connections as well as a three-story multibay frame. Detailed discussions of algorithm performance as well as structural behavior of the resulting optimal designs are given.

Frame Designs

Two multiple-objective optimal design problems were formulated in the companion paper (Foley et al. 2007). A common objective to both formulations was that of minimizing structural member volume. The portal frame formulation sought to maximize confidence in meeting immediate occupancy (IO) and collapse prevention (CP) performance objectives. The constraints in the portal frame optimal design problem included constraints on beam-to-column plastic moment capacity ratios intended to ensure strong column-weak beam (SCWB) behavior and also lower-bound confidence levels. The optimal design problem formulated for multistory frames had additional objectives seeking to minimize the difference between confidence levels associated with column compression force and global interstory drift (balanced confidence objectives). The second optimal design problem formulation was instigated by the results seen in the automated design of the portal frame. Detailed discussion of the reasons for this second formulation for multiple story frameworks will be provided as the results for the portal frame are presented.

A concentrated plasticity approach is used in modeling and plastic hinges are represented as zero-length yielded regions with yielding defined using interaction diagrams appropriate for the member considered. Beam-column members are assumed to have load-moment interaction, while beam members have no load-moment interaction. Foley et al. (2007) provide a graphical illus-

[1]Senior Seismic Research Engineer, John A. Martin & Associates, Inc., 1212 S. Flower St., Los Angeles, CA 90015; formerly, Graduate Student, Univ. of Memphis, Memphis, TN 38152. E-mail: arzhang@johnmartin.com

[2]Emison Professor of Civil Engineering, The Univ. of Memphis, Memphis, TN 38152.

[3]Visiting Associate Professor, Univ. of Wisconsin–Madison, Madison, WI; Associate Professor of Civil Engineering, Marquette Univ., Milwaukee, WI 53233.

Note. Associate Editor: Donald W. White. Discussion open until November 1, 2007. Separate discussions must be submitted for individual papers. To extend the closing date by one month, a written request must be filed with the ASCE Managing Editor. The manuscript for this paper was submitted for review and possible publication on August 26, 2005; approved on April 20, 2006. This paper is part of the ***Journal of Structural Engineering***, Vol. 133, No. 6, June 1, 2007. ©ASCE, ISSN 0733-9445/2007/6-767–776/$25.00.

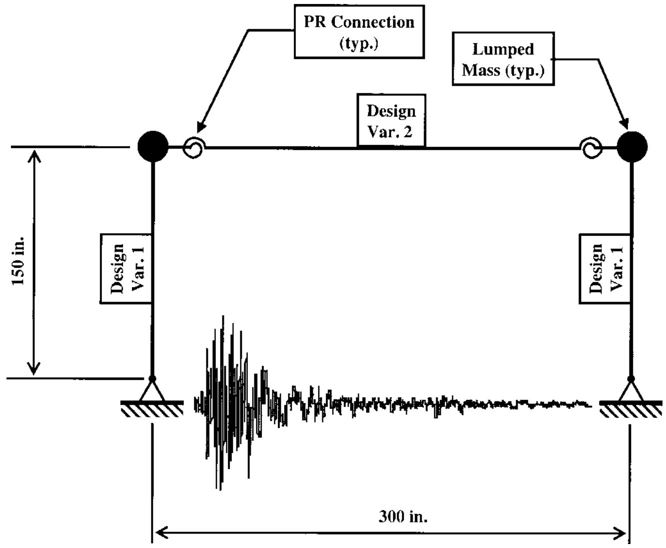

Fig. 1. Portal frame analytical model used in Design Example 1 (1 in.=0.0254 m)

tration of the beam and beam-column interaction surfaces used. Depending on the type of nonlinear model used, each structural element requires a number of parameters by which its inelastic behavior is defined. These parameters are quantities such as positive and negative plastic moment capacities, elastic/inelastic buckling load, and the type of yield surface (force-moment interaction relationships). Nonlinear parameters are in general related to each other and can be defined using the member's cross section, the frame geometry, and the member material properties.

Partially restrained (PR) connections are modeled using a variety of connection properties based on the flexural rigidity and plastic moment capacity of the connected beams. Foley et al. (2007) illustrate the two nonlinear connection types considered in the present study.

All frame designs are evaluated using nonlinear time-history analysis using a suite of 14 ground motions. Seven 50/50 ground motions are used to ascertain if IO performance objectives are being met and seven 2/50 ground motions are used to determine confidence in meeting CP performance objectives. Foley et al. (2007) contain a description of all ground motions used in the present study.

The analytical engine used to evaluate frame designs within the genetic algorithm is DRAIN-2DX (Prakash et al. 1993). The interaction surfaces and connection models described in the companion paper (Foley et al. 2007) were chosen with this analytical engine in mind.

The following sections of the manuscript will provide results and detailed discussions of the application of the genetic algorithm solution to the multiple-objective optimization problems formulated in Foley et al. (2007) for a portal frame with a variety of connection configurations and a multiple-bay, multiple-story moment resisting frame studied previously in the literature.

Portal Frame

The first framework considered is the portal frame shown in Fig. 1. The analytical model for this frame consists of lumped masses at the beam-to-column nodes; pinned supports; and partially restrained connections consisting of zero-length springs. Ground motions are applied in the form of acceleration time histories at the base of the frame as shown. The dimensions for the frame are also provided in Fig. 1. These dimensions reference member centerline dimensions, but rigid offsets were considered without explicit modeling of panel zones' strength and stiffness (Gupta and Krawinkler 1999). The material properties for the members in the frame are: the elastic modulus E=29,000 ksi (200 GPa) and F_y=50 ksi (345 MPa). Lumped mass magnitudes are: 0.085 k s^2/in. (14,885 N s^2/m).

A publicly available genetic algorithm (Carroll 2004) was used in the present study to guide the resizing of design variables during the automated design. The genetic algorithm is carried out with the design represented using two design variables: The first represents the cross section of both columns and the second represents the beam's cross section (Fig. 1). The design variables are taken from a set of 236 possible cross sections of standard AISC beam and column shapes. No special grouping according to beams and columns was done. Structural designs are represented by binary chromosomes that decode to the configuration and structural steel sections used in the frames. In general, a population size of 30 chromosomes with probability of crossover of 60% and probability of mutation of 3.5% were found to produce stable optimization trajectories toward an optimal design solution. Chromosomes of parents reproduce two children chromosomes in generations with 4.0% probability of creep.

The portal frame considered two fully-restrained (FR) beam-end connection configurations as part of special moment resisting frames, and one PR connection configuration within an ordinary moment resisting frame. Additional details regarding the frame configurations denoted using Analysis Case Numbers (ACN) are given in the following:

1. ACN-1: FR connections with SCWB criterion;
2. ACN-2: FR connections with the omission of SCWB criterion; and
3. ACN-3: PR moment connections with SCWB criterion based on the connection's plastic moment capacity. The connection's hysteretic behavior includes inelastic unloading with gap or pinching. The parameters needed to define this connection behavior are provided in the companion paper (Foley et al. 2007).

The initial stiffness and yield moment capacities for the connections are

$$K_c = 10EI/L \tag{1}$$

and

$$M_{cy}^{+} = M_{cy}^{-} = 0.66M_{\mathrm{pb}} \tag{2}$$

The hardening stiffness parameter, α, is defined using a connection rotation of 0.03 rad and a connection moment capacity equal to $1.4M_{cy}$. L=length of the beam; M_{pb}=plastic moment of the beam; and I=second moment of area for the beam.

Fitness trajectories obtained during execution of the GA are shown in Fig. 2. No significant epistatic behavior was observed in the fitness trajectories (each run of the GA resulted in consistent convergence to higher fitness without stagnation). Therefore, the GA parameters appear to have been appropriately chosen for this problem. The average fitness trajectories illustrate that the genetic algorithm is indeed performing search of the design space as exhibited by the fluctuation in the average fitness of the populations with increasing generations.

The portal frame problem consisted of three objectives as outlined in Foley et al. (2007). Slices through objective space (corresponding to objective pairs) for ACN-1 are shown in Figs. 3(a and b). Since 30 chromosomes compete in over 1,000

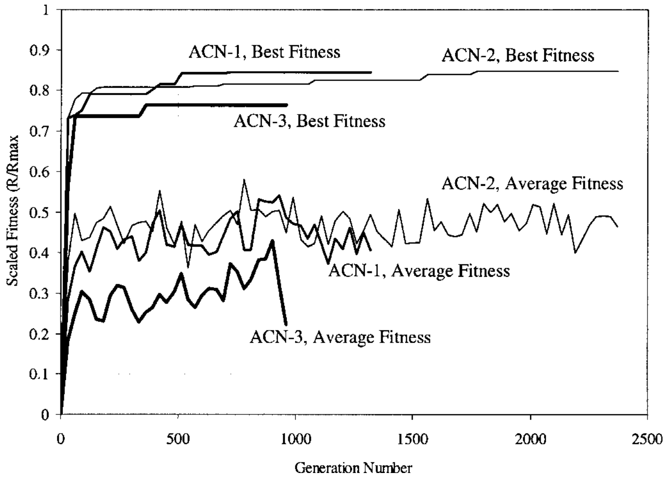

Fig. 2. Fitness trajectories for portal frame with various connections

generations, this figure represents thousands of unique designs. As expected, when the total weight of the structural system decreases, the median interstory drift angle (ISDA) demands increase for IO and CP. These figures illustrate the competing nature of weight and median drift objectives. Fig. 3(c) illustrates that the median estimates of ISDA demand under CP and IO input records appear to be linearly correlated at lower interstory drift ratios (e.g., 0.5% for IO and 1.5% for CP). Higher dispersions were usually observed at higher ranges of nonlinear response demand. Therefore, one might say that satisfying one performance objective for the portal frame could automatically result in the other performance objective being met at certain ranges of nonlinear response (at least for the portal frame and the 14 ground motion records considered). However, as CP demand increases, the correlation is lost and this statement cannot be made.

The radial fitness formulation discussed in the companion paper (Foley et al. 2007) was used in the portal frame and the impact of its use can be seen in Figs. 3(a and b) through the distribution of candidate designs along the Pareto front. The Pareto front can be used by the owner and engineer to understand how confidence in meeting IO and CP performance affects the volume (cost) of the structural system. Obviously, the portal frame is highly simplistic. However, the concept of using multiple-objective optimization algorithms in structural engineering design is highly beneficial.

To understand the difference between three designs (ACN-1 through ACN-3) three frames were chosen from the Pareto front that have roughly equal weight. Pertinent details from these three designs are shown in Table 1. In Table 1, M_{pc}/M_{pb}=ratio of plastic moment capacity of columns to that of the beam; $\mathrm{ISDA}^{\mathrm{PO}}_{\mathrm{median}}$=median interstory drift angle demand at a performance objective (PO)—CP or IO; q^{PO}=confidence level in meeting a defined performance objective; d_{residual}=permanent interstory drift at the end of a component of the Tabas M7.8 (1978) ground motion record; f_1=first-mode natural frequency; ξ_1=first-mode equivalent damping ratio; and G=generation number.

These three designs are different with respect to the ratio of plastic moment capacity of their columns to their girder, but interestingly all of them have very close first-mode natural frequencies, which suggests a strong correlation between displacement responses of such single-mode dominant structures and their first-mode natural frequency. ACN-3 has a slightly shorter first-mode

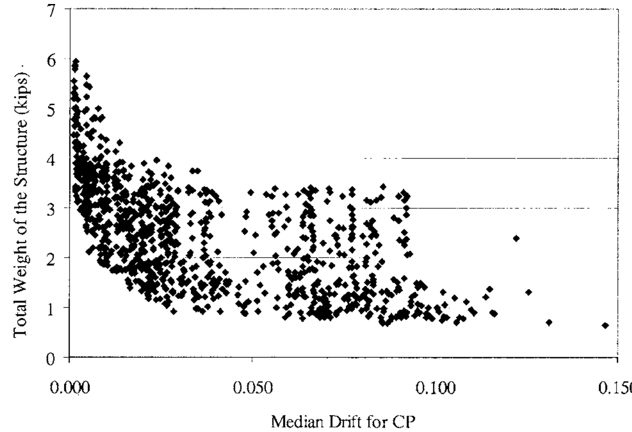

(a)

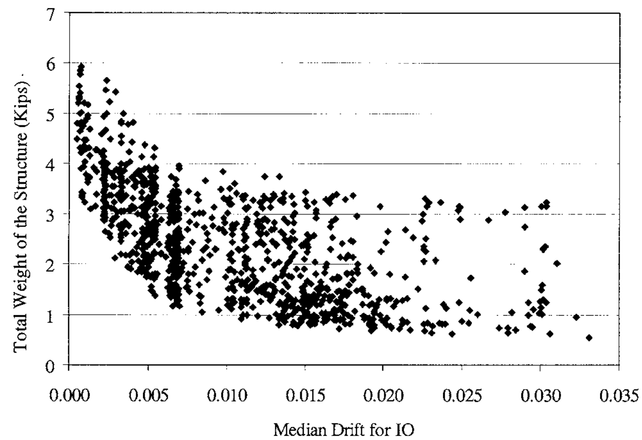

(b)

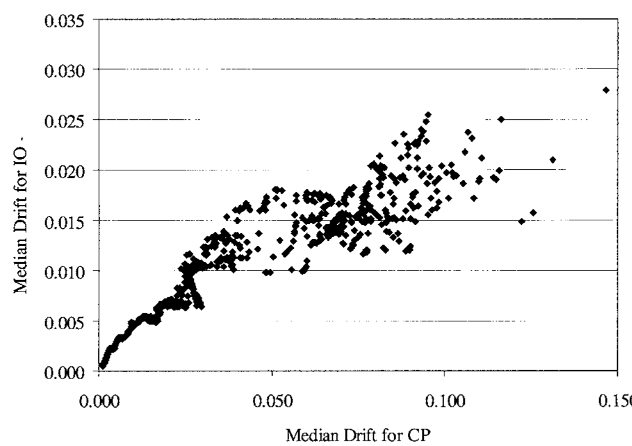

(c)

Fig. 3. Distribution of designs in objective space for portal frame with ACN-1: (a) collapse prevention performance and weight; (b) immediate occupancy performance and weight; and (c) correlation between IO and CP performance objectives (1 kip=4.448 kN; 1 in.=0.0254 m)

frequency that may be attributed to its PR connections. The low IO confidence level of ACN-3 might also be the result of a lower lateral resistance under IO level input motion that can cause lateral deformations to approach the IO capacity faster than CP. Longer natural periods may be advantageous under severe input ground motions provided 10 performance can be met with the added interstory drift that is likely to occur.

Table 1. GA-Generated Designs and Performance Information for the Three Portal Frame Configurations Considered (1 in.^{3}=16.387 $\times 10^{-6}$ m^3)

Parameter	ACN-1	ACN-2	ACN-3
Volume (in.^{3})	14,010	13,830	13,890
Column section	W27×102	W24×55	W27×84
Beam section	W21×57	W21×101	W21×73
M_{pc}/M_{pb}	2.36	0.53	1.42
$\mathrm{ISDA}^{\mathrm{CP}}_{\mathrm{median}}$ (%)	2.06%	2.04%	3.71%
q^{CP} (%)	99.99	99.99	96.78
$\mathrm{ISDA}^{\mathrm{IO}}_{\mathrm{median}}$ (%)	0.70	0.69	0.78
q^{IO} (%)	99.97	99.97	42.10
d_{residual} (%)[a]	0.12	1.09	0.08
R	76.3%	76.6%	76.4%
$\overline{R_{\max}}$	G=44	G=79	G=32
f_1 (Hz)	2.64	2.62	2.40
ξ_1 (%)	4.64	4.61	2.23

[a]Residual ISDA demand at the end of Tabas (1978) ground motion record.

A specific structural volume was chosen for equal weight frames. Then, for this volume, the closest point on the Pareto front with smallest interstory drift represents a near-equal weight design in every analysis case. To evaluate nonlinear static lateral load behavior of the near-equal weight designs (Table 1), pushover curves (displacement-control) were generated. These curves are shown in Fig. 4. A lateral force equivalent to 0.10 g PGA multiplied by the total mass at roof level was applied horizontally. Pushover analyses were performed using a displacement-based procedure. Gravity loads (companion actions) corresponding to the mass magnitude were present. The frame was pushed to a collapse mechanism, or 10 in. of lateral displacement.

Since strong column-weak beam constraint is active in cases ACN-1 and ACN-3, the final designs exhibit beam-type collapse mechanisms with $P-\Delta$ effect after a drift ratio of about 1.5%—the interstory drift angle capacity of low-rise ordinary moment frames at IO performance level is 1% according to SAC (2000). The pushover curves for these connection configurations also show robust monotonic behavior. The lack of available redundancy in the simple portal framework when strong column-weak

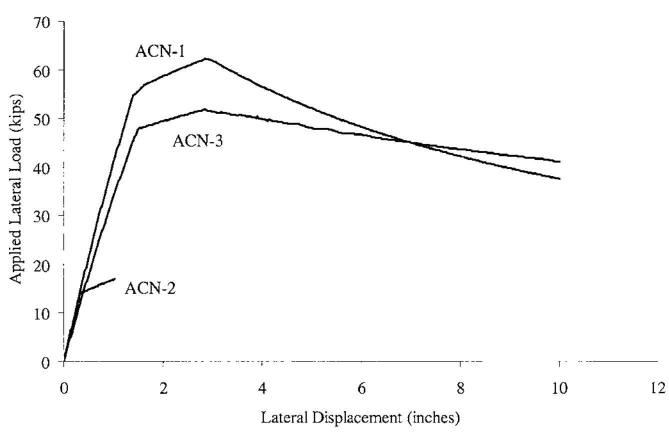

Fig. 4. Lateral force-displacement behavior (pushover response) of equal weight designs (1 kip=4.448 kN; 1 in.=0.0254 m)

Table 2. Connection Types Used in Sensitivity Analysis for Portal Frame

Analysis case number (ACN)	Connection type
1	FR connections with SCWB
2	PR connections (nearly pinned) with SCWB
3	PR connections (flexible) with SCWB
4	PR connections (stiff and strong) with SCWB
5	PR connections (nearly pinned) without SCWB
6	PR connections (flexible) without SCWB
7	PR connections (stiff and strong) without SCWB
8	FR connections without SCWB
9	PR connections (nearly pinned) with SCWB based on the connection's strength
10	PR connections (flexible) with SCWB based on the connection's strength

beam criteria are not considered is shown in the response as well. The pushover curve for ACN-2 has very limited ductility after the initial plastic hinge formation.

To understand how the behavior of different FR/PR moment connections influence the global dynamic response of the optimal structural systems obtained in this study, an optimal design sensitivity analysis for a variety of connection configurations and SCWB criteria was performed. The frame configurations used in the analysis are described in Table 2. In ten analysis cases, connection strength, stiffness, strain hardening ratio, and hysteretic behavior were varied in FR and PR frames. The response of near-equal weight optimal designs was compared. The SCWB criterion could be present or absent in different cases (refer to Table 2). The results of the sensitivity analysis are summarized in Table 3.

Study of response of near-equal weight designs with various connection types and properties in Table 3 reveals the intuitive assumption that stiff and strong connections can reduce lateral deformations in seismic response of regular frames is valid. The reduction in median ISDA (Columns 7 and 8 in Table 3) can be seen as one moves down Table 3 from ACN-2 to ACN-4. Similar behavior is seen with ACN-5 to ACN-7. By using stiff and strong inelastic PR connections (ACN-7) as opposed to flexible PR pinching connections (ACN-6), CP response is reduced by 72%, while IO response is down by 36%. This is a significant improvement for virtually the same amount of structural material used. The SCWB constraint seems to create heavier designs for the same level of performance and as a result, near-equal weight structures without SCWB criterion tend to have a lower displacement response. This can be seen by comparing: ACN-2 with

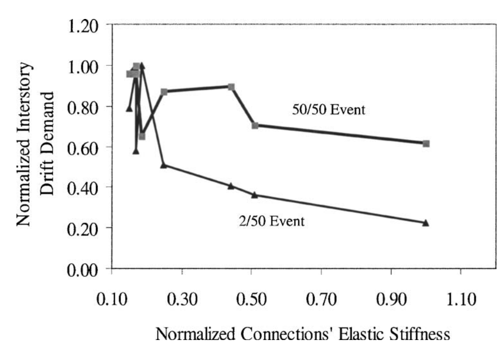

Fig. 5. Variation of interstory drift demand with connection stiffness

Table 3. Summary of the Analyses Results from the Study of Optimal Response Sensitivity to Connections' Behavior (1 in.^{3}=16.387×10^{-6} m^3; 1 lb=4.448 N; 1 in.=0.0254 m)

		Nonlinear connection parameters				Median ISDA (%)			First mode	
ACN	Vol. (in.^{3})	$K_c \times 10^6$ (lb/in.)	α (%)	$M_{cy} \times 10^3$ (lb/in.)	Gap	CP	IO	$R/R_{\max}$	f_1 (Hz)	ξ_1 (%)
1	15,570	463.5	0.050	5.350	No	2.50	0.64	0.736	2.51	4.46
2	16,470	1.745	0.979	4.670	Yes	4.60	0.78	0.446	2.57	3.37
3	16,260	1.547	5.575	5.676	Yes	3.70	0.75	0.724	2.38	3.23
4	15,600	5.307	2.624	9.800	No	1.70	0.55	0.736	2.86	4.42
5	16,230	2.591	0.948	6.732	Yes	2.40	0.68	0.725	2.34	3.63
6	16,230	4.601	4.171	13.04	Yes	1.90	0.70	0.725	2.70	4.21
7	16,230	10.47	1.887	14.15	No	1.05	0.48	0.725	3.51	5.39
8	15,390	773.3	0.015	8.600	No	1.70	0.63	0.740	2.76	4.80
9	16,170	1.929	0.977	5.148	Yes	4.70	0.51	0.725	2.94	3.47
10	16,380	1.769	5.552	6.468	Yes	2.71	0.75	0.722	2.54	3.38

ACN-5; and ACN-3 with ACN-6. It should be noted that lower displacement response, in general, might not be taken exclusively as a good measure of seismic performance, as it may be associated with undesirable patterns of plastic hinge formation in the structure and loss of postyield stability.

The aforementioned interpretations of the FR frames' behavior may also be extended to the response of FR special moment frames in ACN-1 and ACN-8. Here, omission of the SCWB criterion (ACN-8) reduces the CP and IO responses by as much as 32 and 2%, respectively. This response reduction in FR special moment frames is not as significant as in PR ordinary moment frames, which can be attributed to a higher level of integrity of FR special moment frames compared to PR ordinary moment frames.

ACN-9 and ACN-10 utilize the connection's yield moment capacity to evaluate the SCWB criteria rather than the beam's plastic moment capacity as done in the preceding PR analysis cases. The optimal structural design corresponding to ACN-10 lies between systems with and without SCWB criterion. From Table 3, the responses of Cases 9 and 10 are slightly better than Cases 2 and 3 (with SCWB) and worse than Cases 5 and 6 (no SCWB).

Fig. 5 illustrates the variation in normalized interstory drift demand (ISDA) with variation in normalized connection elastic stiffness. Normalization is done with respect to the largest value observed in the analysis set. It is obvious that stiffer moment connections can reduce the lateral deformation response drastically, although IO response seems to be less sensitive to the connections stiffness. Fig. 6 illustrates the variation in normalized ISDA with variation in normalized connection yield strength. As in Fig. 5, it appears that 50/50 response for the optimal designs does not show the same consistent reduction as 2/50 response. The ISDA response did not appear to be sensitive to the connections' hardening ratio in this study.

When studied in the frequency domain, modal properties steadily rise with increase in stiffness of the connections. Variation of the first-mode equivalent damping ratio and natural frequency versus connections' elastic stiffness is plotted in Fig. 7.

Multistory Multibay Moment Resisting Frame

Phase II of the FEMA/SAC project presents several multistory moment resisting frames (MRFs) for use for detailed seismic performance evaluation (FEMA 2000a,b). A three-story four-bay frame shown in Fig. 8 is used as the base topology for application of the proposed automated and optimized design methodology. This frame is a part of seismic resisting system of an office building located in Los Angeles and situated on stiff soil. Ground motion will be considered to be unidirectional and is assumed to be applied in the East-West direction. The MRF considered is located along the southernmost column line in the framing plan. It should be noted that infill framing is assumed to be simply supported and is not shown for clarity. The floors at each level are assumed to act as rigid floor diaphragms and therefore, forces generated during ground motion are assumed to be distributed equally to the perimeter moment resisting frames in orthogonal

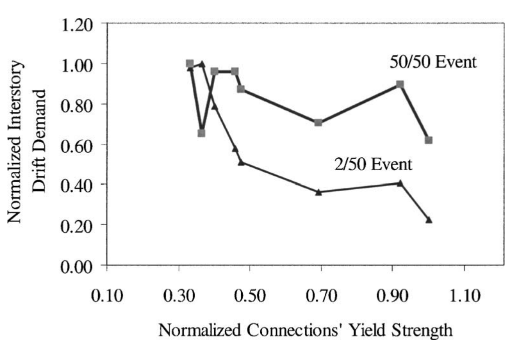

Fig. 6. ISDA versus connection's yield strength

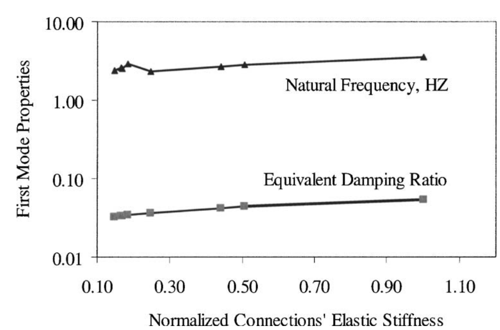

Fig. 7. First-mode properties versus connections' elastic stiffness

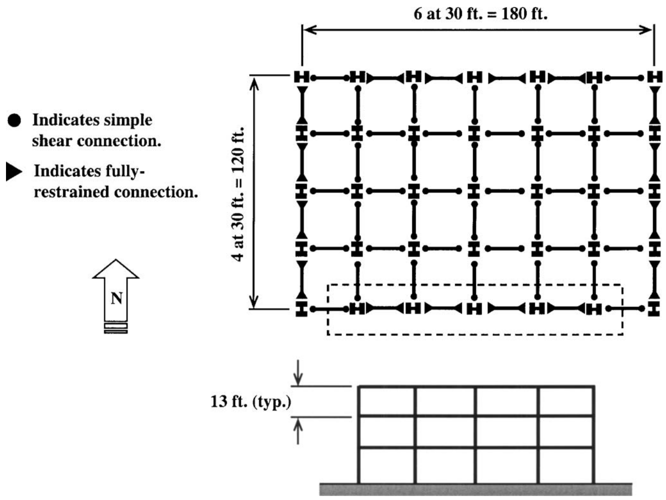

Fig. 8. Plan view and elevation of the multibay multistory example (1 in. = 0.3048 m)

directions. The bases of the columns in the MRF considered were taken to be rigidly attached to the foundation. A leaner column was not used in the analytical model to simulate the destabilizing effect of interior simple framing columns. However, a global second-order nonlinear analysis (material and geometric) that considers the total tributary mass of the building on every lateral resisting frame was implemented for calculation of response.

The loading applied to this frame follows (FEMA 2000b). The floor dead load is taken as $96\ \mathrm{lb/ft^2}$ ($4{,}597\ \mathrm{N/m^2}$) and the reduced live load present when ground motion occurs is taken as $20\ \mathrm{lb/ft^2}$ ($958\ \mathrm{N/m^2}$). The self-weight of the steel framing is taken as $13\ \mathrm{lb/ft^2}$ ($622\ \mathrm{N/m^2}$) and this is assumed to be consistent for all designs generated during the evolution. The seismic mass of the structure at the roof level and floor levels were taken to be: roof—$70.9\ \mathrm{k\,s^2/ft}$ ($12{,}416\ \mathrm{kN\,s^2/m}$); and floors—$65.53\ \mathrm{k\,s^2/ft}$ ($11{,}476\ \mathrm{kN\,s^2/m}$).

There are a significant number of very important assumptions that drove the form of the analytical model used in the DRAIN-2DX (Prakash et al. 1993) analytical engine. Deteriorating stiffness and strength of the hysteresis loops are ignored in this study although recent research results make it possible to conveniently model the deterioration effects of the hysteresis in collapse evaluation (Ibarra et al. 2005). Mass moment of inertia at diaphragm levels is ignored and changes of seismic mass during the time-history analysis are negligible (heavy dead load and live load). Beam-to-column connections are assumed to be fully restrained and panel zone deformations are assumed to be negligible. Finally, soil-structure interaction is ignored.

The multiple-objective optimization problem used to drive the design of the frame considered is based upon the balanced confidence formulation discussed in the companion paper (Foley et al. 2007). The objectives of the problem are to minimize member volume, while seeking to minimize the difference between confidence levels in meeting a performance objective obtained from global interstory drift and column compression force response parameters, at each performance level. Implementation of the genetic algorithm for guiding design variable resizing requires that a fitness function be defined. The balanced confidence formulation essentially recasts the multiple-objective optimization problem into a single fitness statement. The mathematical form of the multiple-objective optimization statement seeking balanced confidence levels and the fitness statement used to execute the genetic algorithm is described in detail in the companion paper (Foley et al. 2007).

Design cases presented here are obtained from a 200-chromosome population size. The convergence criterion is either a minimum of 20 generations without significant improvement of maximum fitness (which is less than 1.0% change in the best fitness of the population after reproduction), or a maximum of 100 generations. None of the design cases required a full 100 generation evaluations in this study. Probability of crossover of 60%, probability of mutation of 2.0%, and 5% probability

Table 4. Final Designs of the SAC Three-Story Frame. Values in Parentheses Are the Constrained Confidence Levels ($1\ \mathrm{in.^3} = 16.387 \times 10^{-6}\ \mathrm{m^3}$).

	Target values		Optimal design					
Design	λ^{CP}_{target} (q^{CP}_{target})	λ^{IO}_{target} (q^{IO}_{target})	$\lambda^{Global\_CP}_{drift}$	λ^{CP}_{CCF}	$\lambda^{Global\_IO}_{drift}$	λ^{IO}_{CCF}	V (in.^{3})	T_1 (s)
1	0.3 (99.9%)	0.3 (99.9%)	0.175	0.305	0.320	0.192	635,227	0.444
2	0.6 (99.0%)	0.3 (99.9%)	0.175	0.305	0.320	0.192	635,227	0.444
3		0.6 (99.0%)	0.585	0.299	0.599	0.221	406,933	0.649
4	0.7 (95.0%)	0.3 (99.9%)	0.163	0.315	0.305	0.201	593,536	0.443
5		0.6 (99.0%)	0.659	0.303	0.617	0.218	333,382	0.730
6		0.7 (95.0%)	0.704	0.174	0.738	0.157	244,282	0.914
7	0.8 (90.0%)	0.3 (99.9%)	0.785	4.779	1.5389	3.778	170,422	1.570
8		0.6 (99.0%)	0.796	7.898	4.779	5.402	177,071	1.510
9		0.7 (95.0%)	0.790	0.203	0.673	0.159	393,156	0.752
10		0.8 (90.0%)	0.757	0.185	0.807	0.123	290,588	0.887
11	0.9 (80.0%)	0.6 (99.0%)	0.871	7.170	1.645	5.392	166,657	1.688
12		0.7 (95.0%)	0.903	15.041	1.745	11.874	157,116	1.558
13		0.8 (90.0%)	0.935	6.483	1.772	5.434	171,708	1.720
14		0.9 (80.0%)	0.903	18.705	1.667	13.465	266,877	1.614
15	1.0 (70.0%)	0.7 (95.0%)	0.999	3.819	1.779	3.524	168,862	1.999
16		0.8 (90.0%)	1.082	5.775	1.618	5.155	132,319	1.884
17		0.9 (80.0%)	1.081	6.039	1.468	4.676	123,828	2.074
18		1.0 (70.0%)	0.985	4.620	1.743	3.860	178,890	1.861

Table 5. Comparison of Results of This Study with Previous Work (1 in.^{3}=16.387×10^{-6} m^3)

Research effort	q^{CP}_{ISDA}	q^{CP}_{CCF}	q^{IO}_{ISDA}	q^{IO}_{CCF}	V (in.^{3})	T_1 (s)
Lee and Foutch (2002)	95%	N.A.	98%	N.A.	265,792	0.86
This study	95%	99.99%	95%	99.99%	244,282	0.91

of creep produced satisfactory results. Chromosomes of parents reproduce two offspring in a tournament selection scheme with elitism.

Binary string chromosomes were used to represent individuals during the evolution. The design variables; however, were grouped in an identical manner to that used by Lee and Foutch (2002). Each chromosome included five genes representing the design variables considered: exterior columns; interior columns; first-floor girders; second-floor girders; and third-floor (roof) girders. Column cross sections were assumed to be uniform from the ground to the roof (no splices in members). The search space includes combinations of 256 AISC W-sections (AISC 2001). No distinction was made between column sections and beam sections in the algorithm. In other words, cross sections that would traditionally be called a beam section (e.g., W33×118) could be used as a column and a cross section traditionally used as a column section (e.g., W14×159) could be used as a beam member. The reason for this is that if columns were limited to W14 series sections, very heavy designs would result. Further, the genetic algorithm employed in the present study would then be able to select from a database of cross-sectional shapes that included those used in FEMA-355F (FEMA 2000a).

A series of 18 design cases were considered. These cases are summarized in Table 4 and were chosen to provide insight into the multiple-objective nature of the problem and interaction between the CP and IO performance objectives. The multiobjective optimization problems are solved through constraining q^{IO} and q^{CP} to key values, while minimizing the objective functions as outlined in the companion paper (Foley et al. 2007). The target confidence levels and corresponding confidence parameters are set such that the final optimal solutions obtained would be distributed at regions of higher importance in the objective space. The prominence of CP performance is first taken into account (Column 2 in Table 4). For each level of CP performance, a variety of IO performance levels are targeted. Naturally, one would not be interested in exploring the performance in the regions of low CP confidence. Similarly, it is not practical or technically appealing to consider designs that have lower IO performance than CP. In other words, design cases were established such that the lowest IO confidence level considered in the series (Column 3 in Table 4) was equal to the target CP confidence level.

Optimal designs resulting from the 18 combinations of CP and IO performance objectives are also shown in Table 4. Several observations can be made based upon the results of design optimization of the second example frame from Table 4. First of all, in higher ranges of CP confidence (at about 99% level), response is principally in the linear elastic regime. Elastic response implies no median permanent lateral deformation in the structure at the end of the application of a set of input ground motion. Linear response implies a linear correlation between median CP and median IO response. Both of these phenomena are evident when one examines a plot of the objective space (similar to Fig. 3 for the portal frame). Therefore, for a given target CP performance parameter, there is a narrow variation of IO performance, if anything at all. In the linear elastic regime, a given CP performance is practically associated with a certain IO performance (Designs 1–3). A wider range in IO performance could be expected as CP target confidence levels drop from 95 to 70% (Designs 4–18). Optimization cases seven and eight show that a design that performs average on CP may not exhibit excellent performance under IO. Cases 11–18 show that a large lateral deformation (above 5.3% ISDA) and average confidence under CP may be naturally associated with low IO confidence. This is because at large lateral displacements, local $P-\Delta$ may be governing the design of columns due to large λ_{CCF} without meeting global collapse.

It is important to note that the computation of the confidence parameter for column compression in FEMA-350 follows the specifications of AISC in which calculation of moment amplification is necessary. This can increase CCF confidence parameter values drastically due to reduced axial compression capacity in the presence of amplified bending moments. Essentially, the frame configuration studied in this example with its current loading conditions would not be able to achieve economic designs with less than 80% level of confidence on having a performance that may be worse than CP with less than 2% probability of exceedance in 50 years.

One should notice that not every single pair of IO and CP structural performance levels could be attained in a weight optimization problem. This is because stiffness and lateral strength of a frame (as well as its ductility and damping) are not continuous variables. When performance for CCF is of concern in addition to

Table 6. Comparison of Final Optimal Design Sections Found Using Proposed Methodology with Design Found in the Literature (FEMA 2000a)

Design case	Exterior columns	Interior columns	First-floor girders	Second-floor girders	Third-floor girders
1	W40×278	W33×318	W27×336	W27×336	W27×336
3	W36×170	W27×336	W21×68	W27×336	W33×118
4	W33×241	W27×336	W36×300	W36×280	W27×336
5	W21×111	W40×264	W12×53	W30×326	W12×79
6	W27×336	W40×149	W16×36	W27×161	W6×15
9	W12×152	W33×221	W18×76	W27×336	W33×201
10	W40×211	W27×178	W10×26	W27×114	W30×235
FEMA-355F	W24×192	W24×207	W24×76	W33×118	W30×108

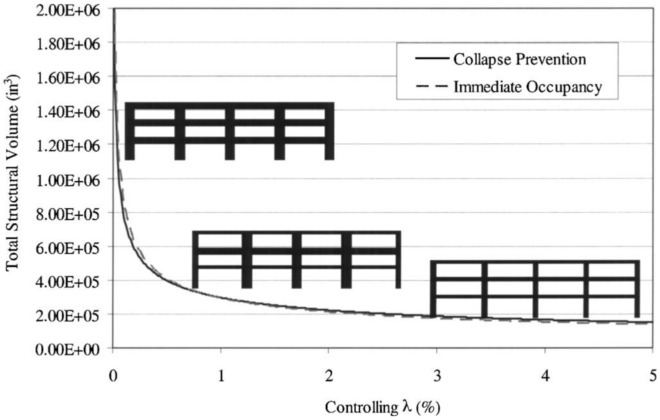

Fig. 9. Final Pareto front for designs of equal IO and CP performance (1 kip=4.448 kN; 1 in.=0.0254 m)

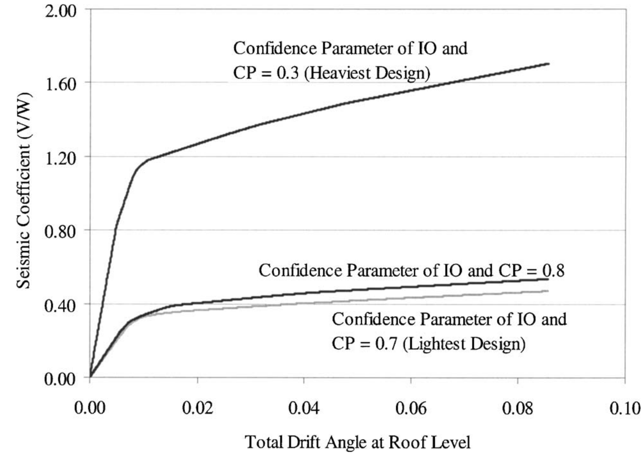

Fig. 11. Displacement-control pushover curves for the final optimal designs

lateral deformations, convergence to an optimal (smallest weight possible) yet structurally stable design may not be feasible at any desired level of performance. The number of pairs of IO and CP performance and the variation they could have from optimizing a structure, in general, depend on:

- Gravitational loading present on the structure;
- Geometrical configuration and redundancy of the lateral resisting systems; and
- Intensity of input ground motion records used in design verification.

As an example, for the SAC frame building studied here, the algorithm could not find a physically viable design that would have 80% level of confidence on meeting a performance level that could be worse than CP with less than 2% probability in 50 years,

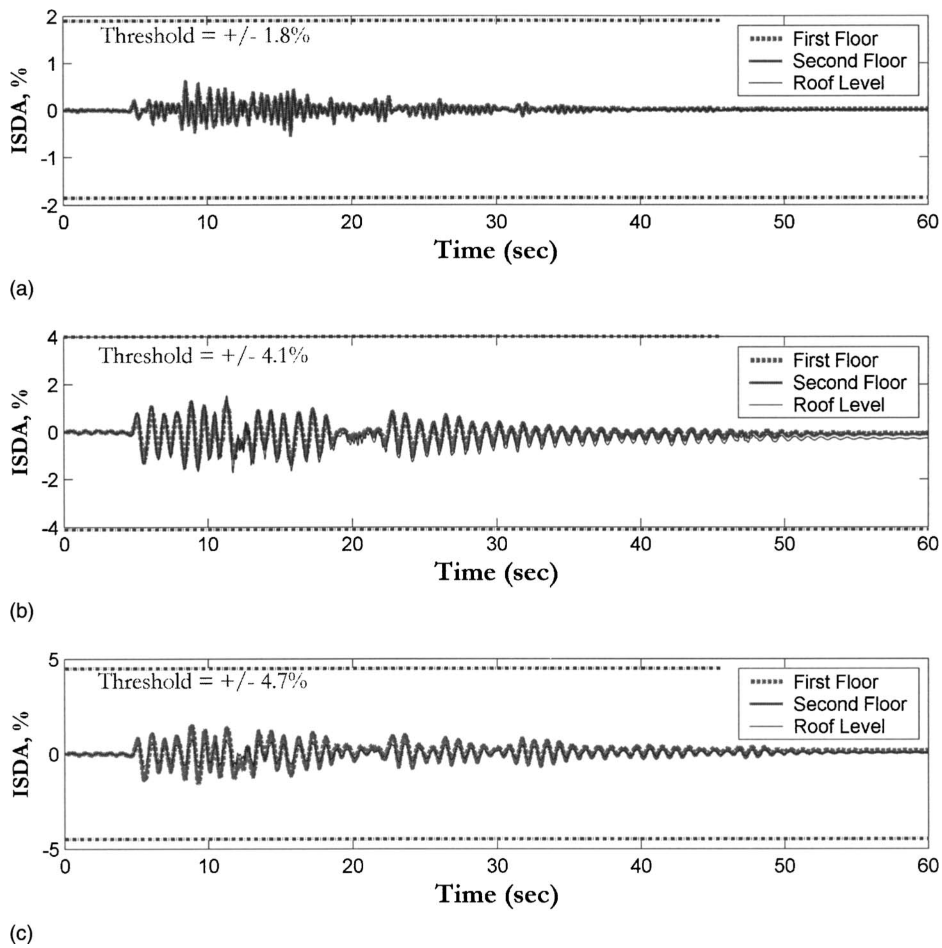

Fig. 10. Sample of ISDA demand histories under Tabas 1978 Iran Earthquake: (a) $\lambda^{CP}=\lambda^{IO}=0.3$; (b) $\lambda^{CP}=\lambda^{IO}=0.7$; and (c) $\lambda^{CP}=\lambda^{IO}=0.8$ (horizontal lines represent the CP ISDA capacity)

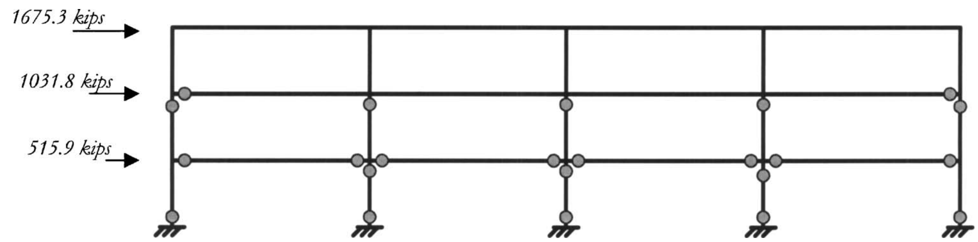

Fig. 12. Plastic hinge formation at confidence parameter CP=IO=0.3 (1 kip=4.448 kN)

and simultaneously meet a 95% level of confidence on having a response that could get worse than IO level with less than 50% probability in 50 years, for the structural configuration, gravity loading, and ground motion suites considered. Designs 7, 8 and 11–18 in Table 4 illustrate that when the frame configuration and target confidence levels get into lower ranges of confidence, it will be very difficult for a designer to attain feasible designs of reasonable weight.

Table 5 presents a comparison between automated designs obtained in this study with one reported in the literature (Lee and Foutch 2002). For the same level of CP and IO performance ($\lambda^{IO}=\lambda^{CP}=0.7$), the optimal design obtained in this study is almost 10% lighter than the one reported by Lee and Foutch (2002). It should also be noted that the method of analysis used in design optimization of this research is nonlinear time-history analysis which results in more accurate estimations of response than static pushover or simplified plastic analysis methods used by Lee and Foutch (2002).

The final optimal design sections for Design Cases 1–10 and those reported in FEMA (2000a) are presented in Table 6. There is consistency between the member sizes found in the present study and those of FEMA (2000a). The use of traditional beam sections as column members in moment resisting frames should be noted. The algorithm used in the present study found that these sections do indeed result in more economical frame configurations, which mirrors current seismic practice. Meeting interstory drift demands could be economically difficult with traditional column sections (e.g., W12, W14 shapes).

Fig. 9 shows Pareto fronts for designs that have equal IO and CP performance. Extraction of frame designs on this front and subsequent curve fitting reveals that the Pareto fronts for IO and CP performance objectives can be expressed as

$$V^{CP} = 10^{-0.418(\log \lambda^{CP})+5.473}$$
$$V^{IO} = 10^{-0.469(\log \lambda^{IO})+5.470} \tag{3}$$

where V^{PO}=volume of the design for performance objective (PO)–IO or CP; and λ^{PO}=controlling confidence parameter at a given PO. One could utilize Eq. (3) to gain a qualifying benchmark for structural volumes that would be required to attain levels of confidence in meeting CP or IO performance objectives. Of course, relationships similar to Eq. (3) would need to be developed for a variety of frame configurations and ground motion suites. However, one could certainly envision utilizing the present algorithm to generate these curves for a series of benchmark frames in various regions of the United States.

Fig. 9 also illustrates that heavier designs result in higher levels of confidence on IO and CP as was expected. For the design criteria and algorithm used, IO level performance for optimal designs was often found to be superior to CP performance. Measures of performance vary with input ground motion characteristics and the mechanical properties of structural systems. The configuration of the SAC three-story frame and the large mass on the frame prevents emergence of designs with a wide variation of confidence levels in Los Angeles.

Fig. 9 is the final product of this study by which economic designs for a given structural system at various ranges of IO and CP performance could be obtained. Having the Pareto surface established for a structural system enables answering questions like: what various pairs of IO and CP performance could result from a range of structural volume for a given CP performance? and how does IO performance change with a change in the structural volume?

To validate the response of optimal structural systems obtained in this example, three of the designs in Table 4 are studied for their time-domain response and lateral pushover capacity in Figs. 10–14. The three systems chosen are Design Cases 1, 6, and 10 in Table 4 corresponding to the following confidence parameter pairs: $\lambda^{CP}=\lambda^{IO}=0.3$; $\lambda^{CP}=\lambda^{IO}=0.7$; and $\lambda^{CP}=\lambda^{IO}=0.8$ corresponding to 99.99, 95, and 90% confidence levels in meeting CP and IO performance, respectively.

Fig. 10 shows the response of these systems under one of the components of the Tabas 1978 (M_w=7.4) Iran earthquake. The horizontal lines in the plots are the threshold ISDA demand at CP level for the constrained confidence parameter in the y axis of the plot. In general, very high confidence in meeting CP and IO performance demanded (e.g., λ=0.3) results in very small interstory drift demand under the Tabas 1978 ground motion. When confi-

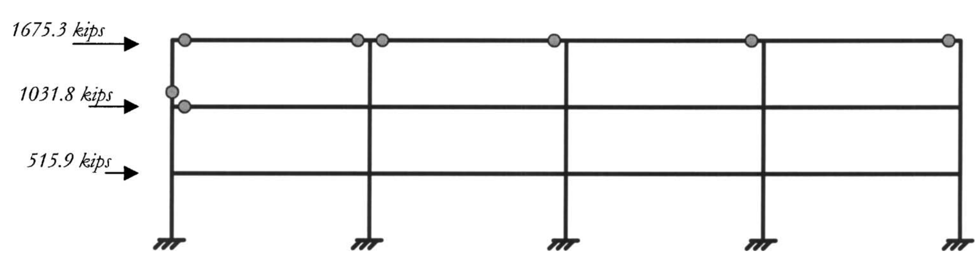

Fig. 13. Plastic hinge formation at confidence parameter CP=IO=0.7 (1 kip=4.448 kN)

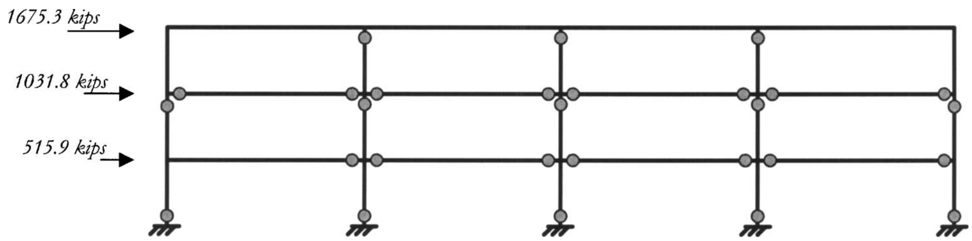

Fig. 14. Plastic hinge formation at confidence parameter CP=IO=0.8 (1 kip=4.448 kN)

dence levels drop, $\lambda^{CP}=\lambda^{IO}=0.7$ and $\lambda^{CP}=\lambda^{IO}=0.8$, response is quite similar except that for the case of confidence parameter of 0.7, ISDA response at the roof level appears to be larger than other floors. The design corresponding to 99.99% confidence in meeting CP and IO performance objectives had no permanent deformation when subjected to Tabas 1978, while the other two confidence levels had negligible permanent drift when subjected to this ground motion.

The pushover response for the three cases is shown in Fig. 11. These displacement-control pushover curves for all designs exhibit a stable behavior without any sign of $P-\Delta$ instability even at large lateral deformations. The frames are subject to a linear distribution of equivalent lateral seismic loads that produce a base-shear equal to the median PGA of CP records times the total seismic mass of the structure. If one considers the common range of seismic design coefficient for this type of frame to be presumably around 0.2 (Lee and Foutch (2002) report a value of around 0.13) the final designs obtained in this example show excellent lateral resistance capacity.

Plastic hinge formation for each of the three cases at a drift angle of 8% (roof relative to ground) is given in Figs. 12–14. No constraints on strong column-weak beam were present during design optimization and this is exhibited by the presence of plastic hinges in the columns. This constraint can be easily added to the design process. It should be noted that the patterns of plastic hinge formation in these figures do not exhibit story-type collapse mechanisms at any level. Further, drift during the ground motions was never at the level of 8% (roof relative to ground) and therefore, these hinge formation patterns were never seen during application of the suites of ground motions considered. Of course, this would have to be validated for a variety of other configurations and ground motion suites than those considered.

Concluding Remarks

The process of using genetic algorithms in design automation of steel moment frames was explained through designing a simple portal frame with different beam to column connections. The optimization statements were evaluated using different sets of constraints to model real-life conditions. It was observed that the median drift demand and the structural performance under CP could generally be enhanced by improving the behavior under IO (and vice versa), whereas improving the behavior for either of the structural performance levels usually results in heavier (and more expensive) designs. Seismic performance evaluation using both interstory drift angle demand and column compression force was considered in optimal designs of a multistory building. Practical considerations in developing a Pareto decision-making surface were discussed. The algorithm is capable of presenting designs with minimum weight that satisfy predefined ranges of preferred seismic performance. A full nonlinear response history analytical engine embedded in the program executes the designs using sets of input ground motion records for maximum accuracy. The computational platform is flexible, relatively fast, and easy to use for practical purposes.

References

American Institute of Steel Construction (AISC). (2001). *Manual of steel construction, load and resistance factor design*, Chicago.

Carroll, D. L. (2004). *FORTRAN genetic algorithm (GA) driver*, CU Aerospace, Champaign, Ill.

Federal Emergency Management Agency (FEMA). (2000a). "State-of-the-art report on performance prediction and evaluation of steel moment frame buildings." *FEMA-355F*, Washington, D.C.

Federal Emergency Management Agency (FEMA). (2000b). "State-of-the-art report on systems performance of steel moment frames subjected to earthquake ground shaking." *FEMA-355C*, Washington, D.C.

Foley, C. M., Pezeshk, S., and Alimoradi, A. (2007). "Probabilistic performance-based optimal design of steel moment resisting frames. I: Formulation." *J. Struct. Eng.*, 133(6), 757–766.

Gupta, A., and Krawinkler, H. (1999). "Prediction of seismic demands for SMRF's with ductile connections and elements." *Rep. No. SAC/BD-99-/06*, Strategic Air Command (SAC) Joint Venture.

Ibarra, L. F., Medina, R. A., and Krawinkler, H. (2005). "Hysteretic models that incorporate strength and stiffness deterioration." *Earthquake engineering and structural dynamics*, Vol. 34, Wiley, New York, 1489–1511.

Lee, K., and Foutch, D. A. (2002). "Performance evaluation of new steel frame buildings for seismic loads." *Earthquake engineering and structural dynamics, Vol. 31*, Wiley, New York, 653–670.

Prakash, V., Powell, G. H., and Campbell, S. (1993). "DRAIN-2DX base program description and user guide, version 1.10." *Rep. No. UCB/SEMM-93/17-18*, Univ. of California–Berkeley, Berkeley, Calif.

SAC. (2000). *FEMA-350: Recommended seismic design criteria for new steel moment-frame buildings*, Federal Emergency Management Agency, Washington, D.C.